

Structural investigation of keV Ar-ion-induced surface ripples in Si by cross-sectional transmission electron microscopy

T. K. Chini*

Surface Physics Division, Saha Institute of Nuclear Physics, 1/AF Bidhannagar, Kolkata 700 064, India

F. Okuyama and M. Tanemura

Graduate School of Engineering, Nagoya Institute of Technology, Gokiso-cho, Showa-ku, Nagoya 466-8555, Japan

K. Nordlund

Accelerator Laboratory, P.O. Box 43, FIN-00014 University of Helsinki, Finland

(Received 4 December 2002; published 6 May 2003)

Using cross-section transmission electron microscopy (XTEM) we have studied the surface and subsurface structure of individual ripples having submicron scale wavelength and nanometer scale amplitude, generated by obliquely incident (50–120 keV) Ar ion bombardment of Si. The XTEM results reveal that the front slopes of ion-induced ripples have amorphous layers containing bubbles with sizes ranging from about 3 to 15 nm facing the ion beam direction. A thinner amorphous layer without bubbles, on the other hand, persists on the rear slope of ripples. We also observe an irregular interface between α -Si and c -Si, which is due to the direct impact amorphization mechanism prevalent near the end-of-range during heavy ion irradiation.

DOI: 10.1103/PhysRevB.67.205403

PACS number(s): 61.80.Jh, 79.20.Rf, 81.16.Rf, 61.50.Ks

I. INTRODUCTION

In recent years, considerable interest has been generated to understand the growth of the periodic wavelike or ripple-like morphology produced on obliquely ion-bombarded solid surfaces.^{1–7} Ion-induced ripples are thought to be produced as a result of the interplay between a roughening process⁸ caused by the erosion (sputtering) of the surface via ion energy dissipation at the subsurface region, and a smoothing process⁹ by thermal or ion-induced diffusion driven by surface energy minimization. Based on this framework, the theoretical approaches^{9–11} usually search for the time evolution of the height function of a nonlinear version of the Kuramoto-Sivashinsky type growth equation. The theory aims to predict the variation of the ripple wavelength/amplitude or surface roughness with ion bombardment parameters such as ion energy, fluence, flux, and angle of ion incidence. Experimentally observed ripple parameters, however, do not always agree with the theoretical predictions. For example, although the theoretically predicted linear variation⁹ of ripple wavelength with ion energy, agrees with experiments only in a few cases^{6,12} one generally observes a power law variation.^{5,7,13} Also, the theoretically predicted amplitude stabilization or rotated ripple structures have been observed experimentally only in rare cases.^{4,14} Thus, studies based on the morphological aspect alone do not seem able to yield a successful theoretical model for ion-induced ripple growth.

Most of the ripple formation experiments have been conducted on semiconductors, such as Si, SiO₂, Ge, and GaAs, though rippling has been observed recently in metals (Ag and Cu) as well.⁴ Amorphization of Si (Refs. 15,16) by heavy ion (such as Ar) bombardment at keV energies occurs in a dose range $\sim 10^{14}$ ions cm⁻² that is much lower than required ($\sim 10^{17}$ ions cm⁻²) for ripples to be observed experimentally. Thus, ripplelike features develop on an amor-

phous matrix in semiconductors, consistent with the basic assumption of the amorphous target in the theoretical models of ion-induced ripple development. However, one can pose the question whether the thickness of the amorphous surface layer really will be uniform, when the surface under bombardment transforms its initially flat geometry to a corrugated one? In a corrugated geometry the local angle of ion incidence does not remain the same on a microscopic scale on the different sides of the ripple waves, so there is no clear reason why the amorphous layer thickness would have to be the same everywhere. This is a very relevant question because quite recently ion-enhanced viscous flow (IVF) (Ref. 7) has been identified as a dominant smoothing mechanism for nanoscale wavelike feature development on (0.5–2.0 keV) Ar ion-eroded SiO₂ surfaces. In IVF the near-surface viscosity is assumed to be confined to a region of constant thickness d extending from the surface towards the bulk within a sinusoidal-shaped amorphous/disordered zone. Chason *et al.*² have also demonstrated that while thermally induced surface diffusion is the primary smoothing mechanism on crystalline surfaces, viscous flow is dominant for amorphous surfaces. Thus, investigation of the crystalline structure of ion-induced ripples is important to provide input to the theoretical studies on the mechanism of ripple growth, as well as to elucidate the basic mechanism of ion solid interaction.

Ripple formation is also potentially interesting from a technological point of view. If the sputter-induced ripple pattern is used for nanoscale wire formation, as proposed in a recent paper,¹⁷ knowledge of the microstructure underlying the ripple morphology is necessary in terms of device performance.

Even though the damage structures of the micron-scale cone-like protrusions grown on ion bombarded solids have been studied extensively using cross-sectional transmission electron microscopy (XTEM) techniques,¹⁸ and a few studies

on ion-induced nanoscale patterns have been performed,^{19,20} there are to our knowledge no studies on the microscopic damage structure of the medium keV heavy ion-induced ripple feature formation. In the present paper we focus on XTEM structural investigation of the ripples produced following Ar ion (50–120 keV) bombardment in Si.

II. EXPERIMENTAL

For ripple generation, small pieces (10 mm×10 mm) of samples cut from a one-side mirror polished, *p* type Si(100) wafer of about 465 μm thickness, were bombarded with focused (typical beam spot of 1.5 mm×2.5 mm) $^{40}\text{Ar}^+$ beam delivered from a 200 keV high current ion implanter (Danfysik) which is described in detail elsewhere.²¹ The angle of ion incidence with respect to the surface normal of the samples was kept at 60°, and the energy of the ion bombardment varied in the 50–140 keV range with a fixed fluence of 10^{18} ions cm^{-2} , while the flux was maintained at $\sim 30\text{--}40 \mu\text{A cm}^{-2}$.

The samples were clamped onto a copper block heat sink, and a negatively biased (−160 V) stainless steel box shielded the target to suppress secondary electrons generated by ion bombardment. The clamping arrangement did not ensure good thermal contact with the copper block. Under the present bombardment parameters, substantial progressive heating of the Si target occurred during irradiation. The rise in temperature was estimated to be around 150–200 °C.

To obtain homogeneous irradiation, the focused beam was scanned with a magnetic *x-y* sweeping system and passed through a circular aperture (diameter of 4 mm) that defined an elliptical beam spot on the sample. The vacuum in the implantation chamber during irradiation remained in the 10^{-7} mbar region. After irradiation, erosion depth was measured with a DEKTAK II profilometer, and the Ar concentration profiles inside a few selected samples with Rutherford Backscattering (RBS).

The morphology of the ion sputtered surfaces was checked by atomic force microscopy (AFM) in contact mode under ambient condition as described earlier.^{13,21} Structural damage of the morphological features developed in the bombarded region was characterized by cross-sectional transmission electron microscopy (XTEM) in a JEM-2000EX (JEOL) TEM operating at 200 keV. The specimens for XTEM were prepared by the standard ion milling technique using Ar^+ beam of 3 keV for prethinning in the first stage and 1.5 keV in the final processing. It should be noted that the structures observed in the TEM and described in this paper are in no case attributable to the action of the ion beam used in the thinning procedure.

III. RESULTS

Figure 1 shows representative AFM images corresponding to the morphology of the samples bombarded by Ar ions at 50 and 120 keV. Ripple topographies clearly visible in the images are oriented perpendicular to the projection of the ion beam onto the surface (arrows indicate ion beam projection). The mean wavelength (l) of the ripples estimated from the

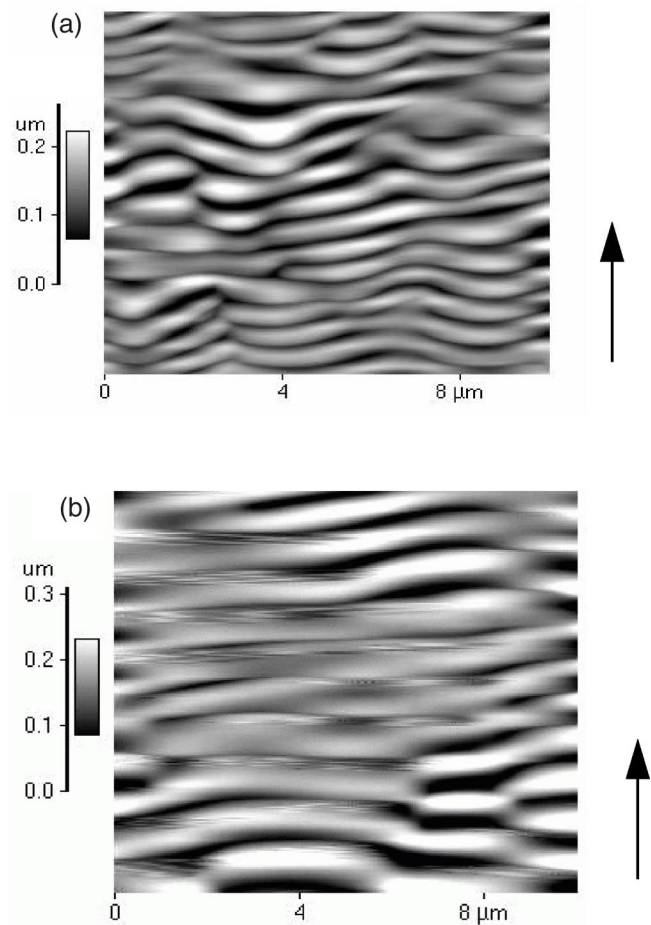


FIG. 1. AFM micrographs of Si bombarded by $^{40}\text{Ar}^+$ at two energies (a) 50 keV and (b) 120 keV. Arrows alongside the micrographs indicate the ripple orientation with respect to the projection of the ion beam.

AFM images under the present experimental condition has been shown in our recent study¹³ to lie in the range $\sim 700\text{--}1000$ nm, while the mean amplitude range was in the 90–140 nm. We have also demonstrated that $l \sim E^{0.45}$ in the ion energy (E) range 50–140 keV.

The same 50 and 120 keV samples observed by AFM were used for XTEM investigation. The XTEM images from low to high magnification of the samples bombarded at 50 and 120 keV are displayed in Figs. 2 and 3, respectively. The sinusoidal-shaped wave pattern of the surface ripples are distinct in the low magnification XTEM images of Fig. 2(a) and Fig. 3(a) (inset). The values of the ripple amplitude and wavelength estimated from the XTEM images are slightly higher than those deduced from the AFM images. This is because the ripple wavelength varies in different parts of the bombarded region, as seen from the representative Fig. 1. Based on many AFM scans taken from different parts of the bombarded region, we have measured the mean wavelength for the 50 keV sample as 680 nm and that for 120 keV as 940 nm (with $\sim 2\%$ uncertainty). The electron-transparent thin regions (prepared by ion milling) of the rippled samples from where the TEM data is taken are quite small, however, and situated at arbitrary locations. For the 50 keV sample the

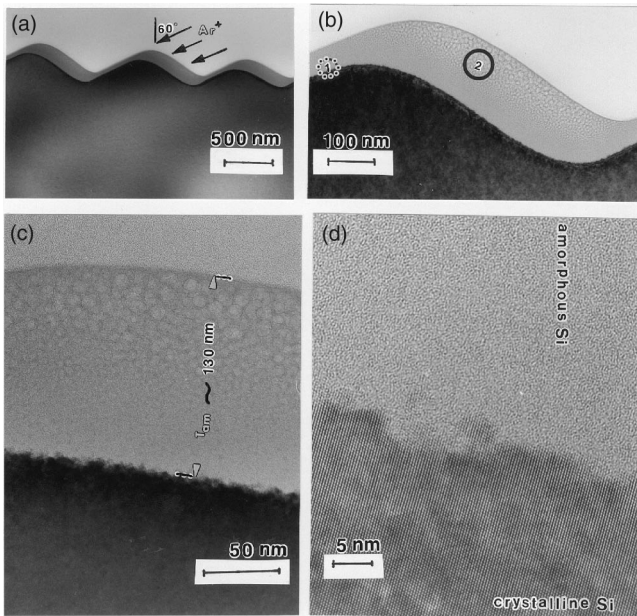


FIG. 2. Cross-sectional TEM image of the Si surface sputtered with a 50 keV $^{40}\text{Ar}^+$ beam. (a) low magnification image and (b) medium magnification image of one of the wave cross-sections from panel (a). (c) High magnification image of the encircled region 1 of panel (b). T_{am} represents the highest thickness of the continuous amorphous surface layer on the front slope with respect to the ion beam. On the front slope cavity/bubble-like features are discernible. (d) HRTEM image of the encircled region 2 of the wave cross section of panel (b). Continuous amorphous phase where $\{111\}$ lattice fringes are clearly observed.

TEM image happens to have been taken from one of the regions of the AFM image (Fig. 1) where the ripple wavelength locally is large. The overall agreement between the AFM and TEM wavelengths for the 120 keV sample is better. The difference in the ripple *amplitude* deduced between the AFM and TEM images may be attributable to the tip convolution effects of AFM.

The outer surface layer of the sinusoidal ripples shows TEM contrast typical of an amorphous phase, which is separated by a thin line of dark contrast from the crystalline bulk phase. That the surface layer is indeed amorphous is confirmed by Fourier transform imaging (not shown here) of a high-resolution (HR) image to be discussed later. The TEM images also indicate that the thickness of the outer amorphous layer of the ripples formed at 120 keV is almost double that at 50 keV. Thus, for the fixed ion dose employed here, the thickness of the amorphous zone at the surface of ripples increases with the energy of the bombarding ion. Interestingly, the thickness of continuous amorphous layer varies over the rippled surface. The amorphous layer on the front slope of the ripple in the ion beam direction is thicker than at the rear slope, as seen in the medium- and high-magnification XTEM images [Figs. 2(b)–3(a) and Figs. 2(c)–3(b)]. The thickness of the amorphous layer on the front slope of the ripple, in the ion beam direction, is ~ 130 and ~ 266 nm at 50 and 120 keV, respectively. The thinner amorphous layer on the rear slope of the ripples at the corresponding energies has a thickness of ~ 54 and ~ 92 nm at

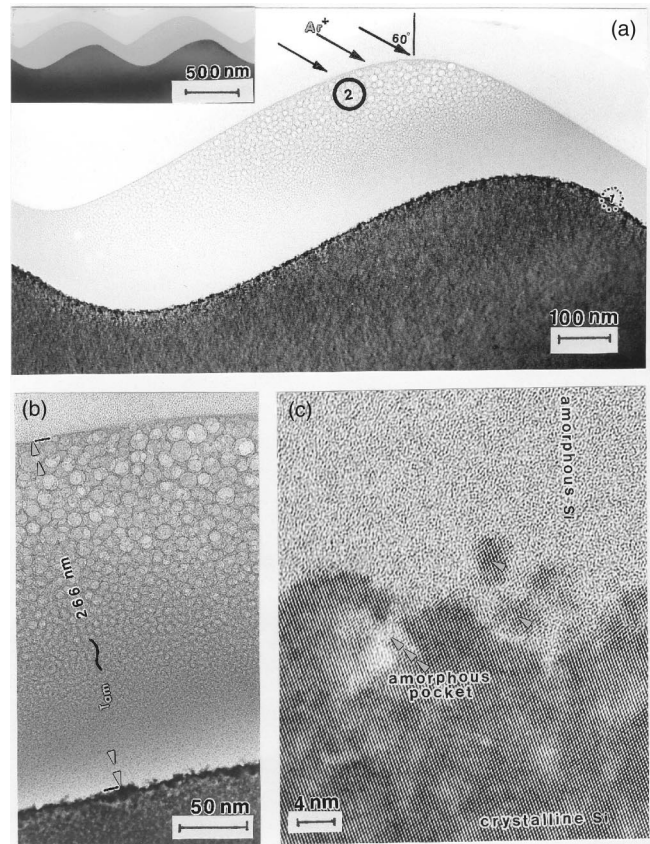


FIG. 3. Cross-sectional TEM image of the Si surface sputtered with 120 keV $^{40}\text{Ar}^+$ beam. (a) medium magnification image of an individual wave. Inset: low magnification image. (b) High magnification image from the encircled region 2 of the wave from panel (a). (c) HRTEM image of the encircled region 1 of the wave cross section of panel (a). Nanocrystallites on the amorphous side of the a/c interface are indicated by arrowheads.

50 and 120 keV, respectively. Formation of such a continuous amorphous zone with variable thickness on the ion-bombarded Si surface has not been reported to date.

Careful inspection of the TEM images [Figs. 2(b)–3(a)] reveals a cavity or porouslike features within the amorphous matrix at the front slope of the ripples. Such features are not prominent on the rear slope. The presence of Ar bubbles in the amorphous phase of the as-implanted Si has been reported^{15,16} in a wide energy region (5–150 keV) even in the moderate dose range 10^{15} – 10^{16} ions cm^{-2} . At the high dose of 10^{18} ions cm^{-2} employed in the present case, most of the cavities are thus believed to be filled with Ar gas and thus are called Ar bubbles hereafter. However, it should be mentioned that for high-dose keV bombardment, the implanted Ar is expected to be present both atomically dispersed and in the form of bubbles.²²

The black encircled region 2 of the single wave cross section from the TEM image of Figs. 2(b) and 3(a) is enlarged in the TEM image of Figs. 2(c) and 3(b) to show that the concentration and size of the bubbles vary with depth while proceeding from the surface towards the amorphous(a)/crystalline(c) interface. The transition region between the presence and the absence of bubbles appears to

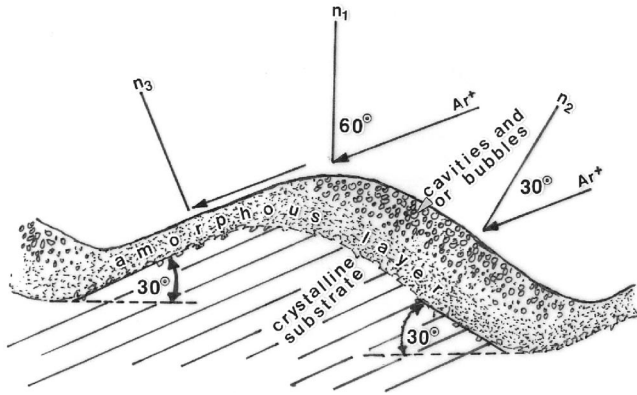


FIG. 4. Schematic diagram showing the structure and morphology of a wave/ripple feature obtained from the TEM images of the present ripple studies.

be more or less sharp for both 50 and 100 keV bombardment. The bubbles exhibited spherical shapes and ranged in diameter from ~ 5 up to ~ 11 nm for the sample at 50 keV Ar bombardment. The maximum bubble diameter is ~ 16 nm at 120 keV bombardment, exhibiting an increasing trend in bubble size with ion energy. The smallest detectable size of the bubbles observed in the present experiment is ~ 3 nm. The overall bubble number density is $\sim 5 \times 10^{11} \text{ cm}^{-2}$.

That the outer layer of ripples is amorphous and the inner core is crystalline was confirmed by high resolution transmission electron microscopy (HRTEM). HRTEM images of the white encircled region 1 from Fig. 2(b) (50 keV Ar bombardment) and Fig. 3(a) (120 keV Ar bombardment) are presented in Figs. 2(d) and 3(c). The $\{111\}$ lattice fringes are distinctly visible in the inner part of the ripples, showing that the crystalline structure of the inner core is the same as that of the substrate silicon. The transition from the amorphous to the crystalline phase is separated by rough interfaces, the roughness being pronounced at higher energy, namely for the sample bombarded at 120 keV. At the (a/c) interface, a few crystalline zones having a dimension of ~ 5 nm or nanocrystallites [shown by arrowheads in Fig. 3(c)] are left on the a -Si side, and a few amorphous pockets of comparable dimension are visible on the c -Si side.

IV. DISCUSSION

We now discuss the structure of the amorphous surface layer. Its complex character, consisting of a near-surface layer with a high density of Ar bubbles as well as an irregular-shaped amorphous-crystalline (a/c) interface at the back side, has to our knowledge not been examined in detail before.

It is first necessary to understand the geometry of the ripples (waves) to be able to understand the underlying structural damage. The ripple geometry can be determined directly from the XTEM images (Figs. 2–3). The ripple cross section shown schematically in Fig. 4 is in the form of a symmetrical triangle with side angles of about 30° (derived directly from the TEM micrograph). This has developed from the initially flat surface when the ion incident angle

with respect to the flat surface normal (n_1 in Fig. 4) was $\theta = 60^\circ$. The direction of the ion beam in Fig. 4 will be reversed for the bombardment at 120 keV. From the ripple geometry, the local ion incidence angles with respect to local surface normals (denoted as n_2 and n_3 in Fig. 4) on the front and rear slope are $\theta_f = (\theta - 30^\circ) = 30^\circ$ and $\theta_r = (\theta + 30^\circ) = 90^\circ$, respectively.

A. Continuous amorphous surface layer with variable thickness and bubble formation

The variation in the penetration depth of the ions, caused by the different local angles of incidence, on the surface of the two slopes of the wave morphology (see Fig. 4) seems to be responsible for the variation in the thickness of the outer amorphous layer.

The observed amorphous thickness can be compared with that calculated from the well known Monte Carlo ion simulator code TRIM (Ref. 23) as follows. For very high fluence heavy ion irradiation such as that used here, the amorphous layer thickness can be estimated from data in Ref. 24 as the maximum of the ion range distribution R_{max} , which is calculated as the mean range plus 3 times the straggling. As the Ar beam angle of incidence is $\sim 30^\circ$ (from Fig. 4) on the front slope of the ripple, the thickness of the amorphous layer on the thicker side can be assumed as $R_{\text{max}} \times \cos(30^\circ)$ (along the local surface normal). On the other hand, on the thinner side (the rear slope of the ripple), the beam comes in almost parallel to the surface. The thickness of the amorphous zone can here be estimated by the radial range of the ions plus 3 times the radial straggling $R_{\text{rad,max}}$.

For 50 keV Ar ions we obtain from TRIM $R_{\text{max}} \times \cos(30^\circ) \approx 110$ nm and $R_{\text{rad,max}} \approx 65$ nm. This compares well with the experimentally observed thickness of the amorphous layers of about 130 and 54 nm on the front and rear slope of the ripples. Similarly, for 120 keV Ar we obtain $R_{\text{max}} \times \cos(30^\circ) \approx 240$ nm and $R_{\text{rad,max}} \approx 130$ nm, which again compares well with the experimental thickness of the amorphous zone of about 270 and 96 nm, respectively. The values for $R_{\text{rad,max}}$ somewhat overestimate the thickness of the rear slope amorphous zone, probably because at grazing incidence many Ar ions are reflected from the surface, thus reducing the effective dose.

We will now discuss the causes of the bubble formation. It is well known that under noble gas ion bombardment of a solid in the keV energy range, the surface is eroded due to the removal of target atoms from the vicinity of the surface by the sputtering process. Simultaneously the projectile is implanted in the subsurface region. There it comes to rest after losing its energy through collisions with target atoms. As the bombardment proceeds, some of the previously implanted noble gas atoms are released from the solid. The sputter-eroded surface eventually reaches the corresponding implanted layer, limiting the retention of the implanted noble gas atoms in the solid. However, after longer exposure to the beam, namely, at high fluence, a steady state or saturation condition is reached when the concentration of implanted atoms remains constant even with further bombardment. For normally incident ion beams, an earlier study²⁵ has estab-

lished that the saturation fluence lies around 10^{17} ions cm^{-2} for the Ar-Si combination in the 10 to 140 keV energy region, and the build-up of a high argon pressure may induce bubble/blister formation. The saturation fluence for an obliquely incident ion beam (as in the present case) is expected to be lower than for a normally incident beam. The total erosion depth was about $3.2 \mu\text{m}$ in the 50 keV case and around $1.3 \mu\text{m}$ in the 120 keV case. This is much more than the thickness of the amorphous zones, indicating that the steady state has indeed been reached. From the RBS measurements of the sputtered area of the present samples we found a nearly Gaussian profile of the implanted Ar atoms. The peak Ar concentration is $\sim 10^{20}$ atoms cm^{-3} located at a depth of ~ 32 nm, while the areal densities of Ar is $\sim 10^{17}$ atoms cm^{-2} in the surface region.

It is well known that Ar has low mobility in Si. Thus, the bubble formation in the present case must have taken place during the bombardment process. The bubble formation can be initiated at vacancies known to exist in irradiated amorphous Si.²⁶ The reason the large size bubbles are localized at a depth shallower than the Ar projected range at the front slope of the ripple is related to the high amount of erosion, which makes the Ar closer to than expected to the surface from a simple range calculation.

An ion beam hitting at $\sim 30^\circ$ with respect to the local surface normal on the front slope of ripple will penetrate deeper in the bulk than the ions hitting the rear slope at near grazing angle. Moreover, as noted above at grazing incidence, a large fraction of the Ar ions are reflected from the surface. As a result, the Ar concentration and hence bubble formation is much more pronounced on the thicker front slope than on the thinner rear slope (Figs. 2–3). That the Ar bubble formation at near grazing ion incidence is reduced has also been reported by another group.¹⁶

B. Amorphous-crystalline (*a/c*) interface

The fact that Si may be rendered amorphous when subject to room temperature keV energy Ar irradiation is well known in the field of ion-solid interaction research. However, the nature of the amorphous-crystalline (*a/c*) interface produced is a key factor to explain the mechanism of amorphization prevalent in a particular bombardment condition. Ar ions with keV energies can directly amorphize fairly large regions of Si in a collision cascade induced by a single ion.^{27–30} From comparison with previous molecular dynamics simulations,³⁰ we estimate that an amorphous zone produced by a single Ar ion in a single subcascade can have an average diameter on the order of ~ 3 nm, and in one dimension be at least 5 nm in size. An Ar ion with energies exceeding 20 keV will produce several amorphous zones in individual subcascades, most of which are spatially well separated [compare, e.g., with Fig. 3 in Ref. 30 and Fig. 3(b) in Ref. 29].

The amorphization of Si proceeds usually both by direct impact and defect stimulated amorphization.³¹ However, in the case of fairly heavy ions such as Ar, the direct impact amorphization mechanism will dominate close to the end of the ion range. The features seen at the interface in the TEM images for 50 and 120 keV Ar irradiation, Figs. 2(d) and

3(c), can thus be understood in a direct impact amorphization picture. The interface is formed near the end-of-range of the Ar ions. Each Ar ion will produce a few amorphous zones. The amorphization will then proceed in a stochastic manner: amorphous pockets are produced at random locations near the interface, so instead of a sharp interface, one is left with an irregular one. A few crystalline zones are left on the *a*-Si side, and a few amorphous pockets (produced by the individual ions with the deepest penetration) have been produced on the *c*-Si side. The size of the amorphous zones in Fig. 3(c) corresponds well to the size of the amorphous regions seen in MD simulation, 3–5 nm.

At implantation doses higher than 10^{16} ions cm^{-2} , recrystallization is known to occur at temperatures higher than room temperature.³² However, the estimated temperature rise during the present bombardment condition (mentioned in the experimental section) is much less than the $550\text{--}600^\circ\text{C}$ required to recrystallize³³ the continuous amorphous layer produced by the bombardment. Moreover, Cullis *et al.*³⁴ demonstrated that large quantities of Ar present in a damaged Si layer, as in the present experimental situation, can suppress the recrystallization.

V. CONCLUDING REMARKS

In summary, using cross-sectional transmission electron microscopy (XTEM), a continuous amorphous layer extending far beyond the mean penetration depth of the ions has been observed in Si on the surface of the sinusoidal ripples produced by 50–120 keV argon bombardment at 60° incident angle. The amorphous layer on the front slope of the sinusoid facing the beam direction is much thicker than the amorphous layer residing on the opposite slope. Moreover, the thicker amorphous side is embedded with nanometer-sized bubbles. The irregular-shaped interface between *a*-Si and *c*-Si gives evidence that the direct impact amorphization mechanism is dominant for obliquely incident high-dose argon bombardment of silicon in the 50–120 keV ion energy range.

However, it is not clear how the local angle of ion incidence settles at a value differing by about 30° from the initial large angle of ion incidence in the present experiment. Additional studies on the damage structure evolution of the obliquely bombarded silicon as a function of bombardment time or fluence will be needed to understand the growth mechanism of the ion induced ripple itself, as well as the thickness variation of the disordered layer and bubble formation.

ACKNOWLEDGMENTS

T.K.C. acknowledges the generous financial support from the Association of International Education, Japan (AIEJ) for his short term visit to the Nagoya Institute of Technology, Japan for the XTEM work. He thanks Professor M. K. Sanjal and Professor S. R. Bhattacharyya for their encouragement in this work. T.K.C. also thanks Mr. Subir Roy, Mr. Abhijit Das, Mr. Souvik Banerjee, Mr. Chandan Roy, and Mr. Samir Basak of the Surface Physics Division for their

technical assistance, Mr. Satyabrata Mahapatra of the Institute of Physics, India for the RBS work and Mr. Tadanori Yoshioka of JEOL Hightech Co., Ltd., Japan for his competent assistance in TEM work. K.N. acknowledges financial

support from the Academy of Finland under Project No. 46788 and M.T. appreciates financial support from the Japan Society for the Promotion of Science (JSPS) under Grants-in-Aid for Scientific Research B, No. 12450038.

*Electronic address: tapashp@hp2.saha.ernet.in

- ¹G. Carter and V. Vishnyakov, Phys. Rev. B **54**, 17 647 (1996).
- ²E. Chason, T. Mayer, B. K. Kellerman, D. T. McIlroy, and A. J. Howard, Phys. Rev. Lett. **72**, 3040 (1994); T. M. Mayer, E. Chason, and A. J. Howard, J. Appl. Phys. **76**, 1633 (1994).
- ³J. Erlebacher, M. J. Aziz, E. Chason, M. B. Sinclair, and J. A. Floro, Phys. Rev. Lett. **82**, 2330 (1999).
- ⁴S. Rusponi, C. Boragno, and U. Valbusa, Phys. Rev. Lett. **81**, 2735 (1998).
- ⁵S. Habenicht, W. Bolse, H. Feldermann, U. Geyer, H. Hofsass, K. P. Lieb, and F. Roccaforte, Europhys. Lett. **50**, 209 (2000).
- ⁶A. Dutta, Y. R. Wu, and Y. L. Wang, Phys. Rev. B **63**, 125407 (2001).
- ⁷C. C. Umbach, R. L. Headrick, and K. C. Chang, Phys. Rev. Lett. **87**, 246104 (2001).
- ⁸R. M. Bradley and J. M. E. Harper, J. Vac. Sci. Technol. A **6**, 2390 (1988).
- ⁹M. A. Makeev and A. L. Barabasi, Appl. Phys. Lett. **71**, 2800 (1997); M. A. Makeev, R. Cuerno, and A. L. Barabasi, Nucl. Instrum. Meth. B **197**, 185 (2002).
- ¹⁰R. Cuerno and A. L. Barabasi, Phys. Rev. Lett. **74**, 4746 (1995).
- ¹¹S. Park, B. Kahng, H. Jeong, and A. L. Barabasi, Phys. Rev. Lett. **83**, 3486 (1999).
- ¹²D. Flamm, F. Frost, and D. Hirsch, Appl. Surf. Sci. **179**, 95 (2001).
- ¹³T. K. Chini, M. K. Sanyal, and S. R. Bhattacharyya, Phys. Rev. B **66**, 153404 (2002).
- ¹⁴J. Erlebacher, M. J. Aziz, E. Chason, M. B. Sinclair, and J. A. Floro, J. Vac. Sci. Technol. A **18**, 115 (2000).
- ¹⁵P. Revesz, M. Wittmer, J. Roth, and J. W. Mayer, J. Appl. Phys. **49**, 5199 (1978).
- ¹⁶U. Bangert, P. J. Goodhew, C. Jeynes, and I. H. Wilson, J. Phys. D **19**, 589 (1986).
- ¹⁷J. Kim, B. Kahng, and A. L. Barabasi, Appl. Phys. Lett. **81**, 3654 (2002).
- ¹⁸F. Okuyama and J. Kato, Surf. Sci. **338**, L857 (1995), and references therein.
- ¹⁹R. Gago, L. Vazquez, R. Cuerno, M. Varela, C. Ballesteros, and J. M. Albella, Appl. Phys. Lett. **78**, 3316 (2001).
- ²⁰S. Facsko, T. Dekorsy, C. Koerdt, C. Trappe, H. Kurz, A. Vogt, and H. L. Hartnagel, Science (Washington, DC, U.S.) **285**, 1551 (1999).
- ²¹T. K. Chini, D. Datta, S. R. Bhattacharyya, and M. K. Sanyal, Appl. Surf. Sci. **182**, 313 (2001).
- ²²H. A. Filius, A. Vanveen, K. R. Bijkerk, and J. H. Evans, Radiat. Eff. Defects Solids **108**, 1 (1989).
- ²³J. F. Ziegler, J. P. Biersack, and U. Littmark, *The Stopping and Range of Ions in Solids* (Pergamon, New York, 1985), and also available from the website www.srim.org
- ²⁴K. Nordlund, J. Keinonen, E. Rauhala, and T. Ahlgren, Phys. Rev. B **52**, 15 170 (1995).
- ²⁵K. Wittmaack, P. Blank, and W. Wach, Radiat. Eff. **39**, 81 (1978).
- ²⁶S. Roorda, R. A. Hakvoort, V.-A. Van, P. A. Stolk, and F. W. Saris, J. Appl. Phys. **72**, 5145 (1992).
- ²⁷M. O. Ruault, J. Chaumont, J. M. Penisson, and A. Bourret, Philos. Mag. A **50**, 667 (1984).
- ²⁸I. Jencic and I. M. Robertson, J. Mater. Res. **11**, 2152 (1996).
- ²⁹M. -J. Caturla, T. D. Rubia, L. A. Margus, and G. H. Gilmer, Phys. Rev. B **54**, 16 683 (1996).
- ³⁰K. Nordlund, M. Ghaly, R. S. Averback, M. Caturla, T. D. Rubia, and J. Tarus, Phys. Rev. B **57**, 7556 (1998).
- ³¹J. Nord, K. Nordlund, and J. Keinonen, Phys. Rev. B **65**, 165329 (2002).
- ³²J. S. Williams, R. D. Goldberg, M. Petravic, and Z. Rao, Nucl. Instrum. Methods Phys. Res. B **84**, 199 (1994).
- ³³F. F. Morehead, Jr. and B. L. Crowder, Radiat. Eff. **6**, 27 (1970).
- ³⁴A. G. Cullis, T. E. Seidel, and R. L. Meek, J. Appl. Phys. **49**, 5188 (1978).